# Experimental Study of Fluidization of 1G-Geldart D-Type Particles in a Rotating Fluidized Bed with a Rotating Chimney

**Juray De Wilde and Axel de Broqueville**
Dept. of Materials and Process Engineering, Université Catholique de Louvain, Réaumur, Place Sainte Barbe 2, 1348-Louvain-la-Neuve, Belgium

*DOI 10.1002/aic.11532*
*Published online June 4, 2008 in Wiley InterScience (www.interscience.wiley.com).*

*The new concept of a rotating chimney for rotating fluidized beds is experimentally investigated using a step-response technique. The chimney rotates in the same sense as the rotating particle bed, but not necessarily at the same rotational speed. In particular, chimney rotational speeds such that the particles at contact with the chimney obtain a rotational speed higher than the average particle bed rotational speed are possible. The increase of the centrifugal force in the vicinity of the chimney allows to reduce solids losses via the chimney and to build up a higher solids loading in the fluidization chamber at given fluidization gas flow and solids feeding rates. Alternatively, at given solids loading and fluidization gas flow rate, the rotating chimney allows to control the particle residence time in the fluidization chamber. The influence of the chimney rotational speed and the fluidization gas flow rate is studied using 1G-Geldart D-type particles.* © 2008 American Institute of Chemical Engineers *AIChE J,* 54: 2029–2044, 2008

*Keywords: fluidization, particle technology, particulate flows*

## Introduction and Concept

In conventional fluidized beds, earth gravity is balanced by the gas–solid drag force. The role of earth gravity determines and limits the flow regimes and operating conditions of conventional fluidized beds.[1] In particular, the gas–solid slip velocity and the related gas–solid mass and heat transfer can be limited, for example obliging to limit the catalyst activity for very fast, highly endothermic or exothermic catalytic reactions. To overcome the limitations related to earth gravity, different alternative fluidization techniques have been proposed. The two most important techniques are fluidization in a magnetic field[2] and fluidization in a centrifugal field.[3–7] The present work addresses the latter. Fluidization in a centrifugal field has been investigated since the seventies using so-called rotating fluidized beds, referred to as conventional rotating fluidized beds in the present work.[3–11] In conventional rotating fluidized beds, radial fluidization of a cylindrically shaped particle bed is obtained by balancing a centrifugal force introduced by rotating the fluidization chamber fast around its axis of symmetry by means of a motor and a radial gas–solid drag force introduced by feeding the fluidization gas through multiple radial gas inlets in the outer cylindrical wall of the fluidization chamber and forcing the fluidization gas to leave the fluidization chamber via a centrally positioned chimney.[3–11] Centrifugal forces much higher than gravity can be imposed, allowing to increase the gas–solid slip velocity and to improve the gas–solid mass and heat transfer.[8] Furthermore, the Geldart classification of particles shifts as a function of the centrifugal force that is imposed.[9] This way, sufficiently high centrifugal forces allow to fluidize particles that cannot be fluidized in the earth gravity field, as for example cohesive 1G-Geldart C-type particles.[9–11] Conventional rotating fluidized beds pose major challenges with respect to sealing and mechanical vibrations. To eliminate those challenges, while still taking advantage of fluidization in a centrifugal field, the concept of a rotating fluidized bed in a static geometry has been recently presented.[12,13] In

Correspondence concerning this article should be addressed to J. De Wilde at juray.dewilde@uclouvain.be.

rotating fluidized beds in a static geometry, the rotating motion of the particle bed is introduced by the tangential injection of the fluidization gas in the fluidization chamber by multiple gas inlet slots in the outer cylindrical wall of the fluidization chamber. First experimental observations showed that a uniform rotating fluidized bed could be obtained, provided that the solids loading was sufficiently high.[12] At too low solids loadings, channeling and slugging were observed.[12] The influence of the fluidization gas flow rate on channeling and slugging was less clear. Solids losses via the chimney may prevent a sufficiently high solids loading to build up. Therefore, solids losses via the chimney have to be minimized. In this context, the new concept of a rotating chimney[14] is presented and experimentally investigated using a dual step-response technique.

The rotating chimney (Figures 1a, b) consists of multiple blades with openings to the chimney in between and rotates in the same sense as the rotating particle bed, but not necessarily at the same rotational speed.[14] In particular, chimney rotational speeds such that the particles at contact with the chimney obtain a rotational speed higher than the average particle bed rotational speed are possible. In such case, the rotating chimney can significantly increase the centrifugal force in the vicinity of the chimney. Whereas the fluidization gas is forced to leave the fluidization chamber via the chimney, the increased centrifugal force in the vicinity of the chimney prevents the particles to be entrained by the gas to the chimney. By the action of the centrifugal force, particles entrained by the gas to the vicinity of the chimney are returned to the rotating particle bed against the outer cylindrical wall of the fluidization chamber. Furthermore, particles entrained to the chimney via its one open end can be returned to the fluidization chamber by the action of the centrifugal force via the openings in between the chimney blades (Figure 1b). To allow this, the central fixed chimney tube toward the cyclone and filter bag (see Ref. 12) is inserted half way down the fluidization chamber. Alternatively, a rotating chimney with two closed ends could be used.

The new concept of fluidization in a centrifugal field around a rotating chimney is as such introduced. Whereas the radially outwards centrifugal force is generated by the rotating motion of the chimney, the radially inwards gas–solid drag force is introduced by feeding the fluidization gas outside the chimney and forcing it to leave via the chimney. The balance or imbalance between the two opposing forces can be controlled via the fluidization gas flow rate and the chimney rotational speed. It should be remarked that the effect of the rotating chimney is expected to be quite local, that is, limited to the vicinity of the chimney. In this context, the combination of the rotating chimney with another fluidization technique, for example, the rotating fluidized bed in a static geometry,[12] should be kept in mind and is considered in this work.

By reducing or eliminating solids losses via the chimney, higher solids loadings in the fluidization chamber can be built up. As shown by De Wilde and de Broqueville,[12] high solids loadings may be essential to obtain a uniform rotating particle bed, without channeling or slugging. This is investigated in more detail in the present work.

In the analysis that follows and based on a solid body type rotation of the particle bed, the average particle bed rotational speed $\langle \tilde{\omega}_{\text{bed}} \rangle$ in radians per second (radps) will be used. Assuming the distance from the particle bed freeboard to the rotating chimney to be sufficiently large to be able to

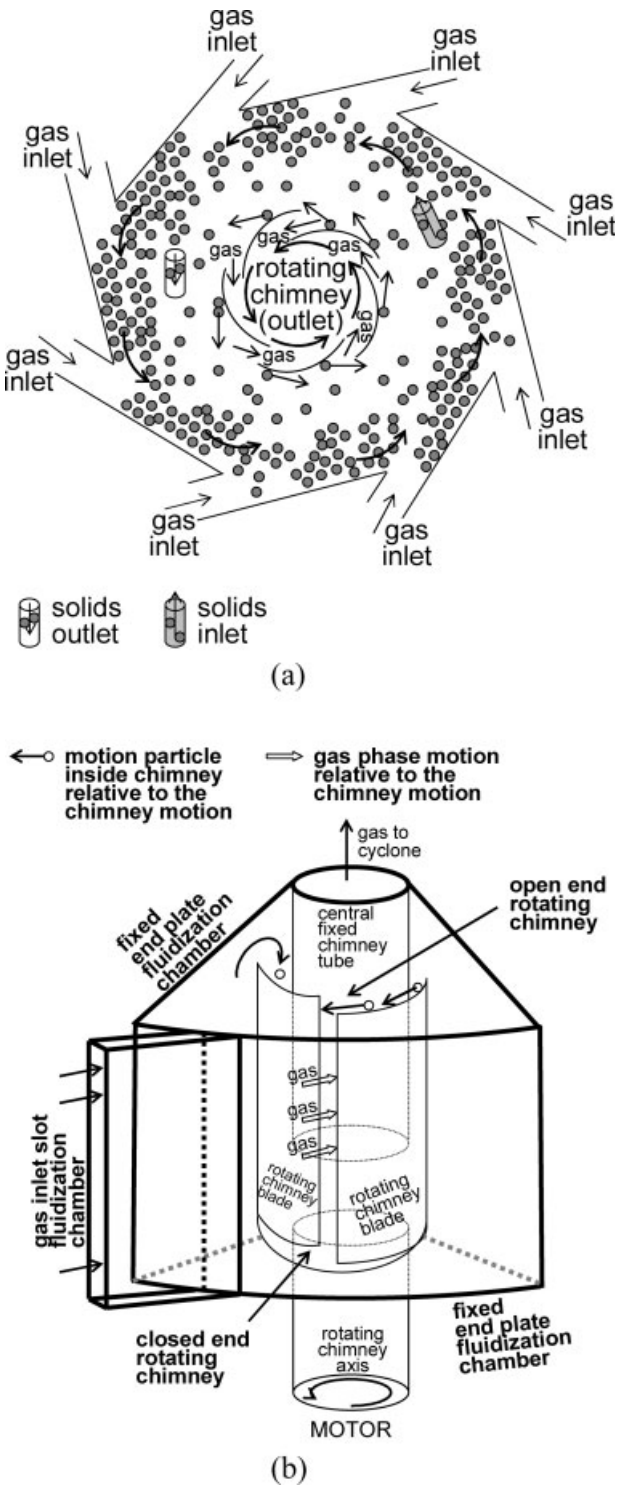


**Figure 1. Schematic representation of a rotating chimney in a rotating fluidized bed.**

(a) 2D Cross section showing absolute velocities (qualitatively); (b) Partial 3D view showing velocities relative to the chimney motion (qualitatively).

neglect the effect of the rotating chimney on the average rotating particle bed motion, the average particle bed rotational speed in radps can be estimated from:

$$\langle \tilde{\omega}_{\text{bed}} \rangle = \langle v_{\text{tan g}} \rangle / \langle r_{\text{fluid.chamber}} \rangle, \quad (1)$$

where $\langle r_{\text{fluid. chamber}} \rangle$ is the average fluidization chamber radius:

$$\langle r_{\text{fluid.chamber}} \rangle = (R^{\text{outer}}_{\text{fluid.chamber}} + R_{\text{chimney}})/2, \quad (2)$$

and $\langle v_{\text{tan g}} \rangle$ is the average tangential particle bed velocity:

$$\langle v_{\text{tan g}} \rangle = \tilde{G} \cdot s^{\text{gs}}_{\text{tan g}} \cdot \langle n^{\text{rotations}}_{\text{g}} \rangle / ((R^{\text{outer}}_{\text{fluid.chamber}} - R_{\text{chimney}}) \cdot \varepsilon^{\text{bed}}_{\text{g}} \cdot L_{\text{fluid.chamber}}). \quad (3)$$

In Eq. 3, $\tilde{G}$ is the total fluidization gas flow rate in cubic meters per second and $s^{\text{gs}}_{\text{tan g}}$ is the tangential gas–solid slip factor in the rotating particle bed $\langle v_{\text{tan g}} \rangle / \langle u_{\text{tan g}} \rangle$. The latter is determined by the balance between the tangential gas–solid drag force and the shear in the rotating particle bed due to particle–particle and particle-wall collisions. $\langle n^{\text{rotations}}_{\text{g}} \rangle$ is the average number of rotations of the gas in the fluidization chamber. In the absence of particles, the average number of rotations of the fluidization gas in the fluidization chamber can be larger than 1. In the presence of particles, however, the gas is facing the resistance of a particle bed. As a result, in the presence of particles, the average gas phase tangential velocity in the fluidization chamber is expected to decrease and the fluidization gas is expected to leave the fluidization chamber after a reduced number of rotations in the fluidization chamber. The fluidization gas, being injected tangentially (Figure 1a) and also facing the resistance of a particle bed in the radial direction, is expected to follow a curved flow path toward the chimney, resulting in an average number of rotations of the fluidization gas in the fluidization chamber smaller than 1. As will be experimentally demonstrated further in this article, within a certain fluidization gas flow rate range, $s^{\text{gs}}_{\text{tan g}}$ and $\langle n^{\text{rotations}}_{\text{g}} \rangle$ can be assumed to be independent of the fluidization gas flow rate and, hence, $\langle v_{\text{tan g}} \rangle$ and $\langle \tilde{\omega}_{\text{bed}} \rangle$ can be assumed to increase proportionally with the fluidization gas flow rate (Eqs. 1 and 3).

In what follows, a tangential particle-chimney slip factor $s^{\text{sc}}_{\text{tan g}} = \langle v^{\text{particle at chimney}}_{\text{tan g}} \rangle / \langle v^{\text{chimney}}_{\text{tan g}} \rangle$ will also be introduced which accounts for the slip between the rotating chimney and the particles at contact with the chimney. As a result of the latter, the rotating chimney cannot transfer all of its tangential momentum to the particles at contact with the chimney which will be rotating at the tangential particle-chimney slip factor times the chimney rotational speed.

It should be remarked that in the figures shown in this work, the average particle bed and chimney rotational speeds $\langle \omega_{\text{bed}} \rangle$ and $\langle \omega_{\text{chimney}} \rangle$ in rotations per minute (rpm) and the fluidization gas flow rate $G$ in normal cubic meters per hour are used.

## Experimental Set-Up

The concept of the rotating chimney and its influence on a rotating fluidized bed is experimentally investigated using a dual step-response technique, illustrated in Figure 2. The responses of the rate of solids losses via the chimney and of the pressure drop over the fluidization chamber to step changes in the solids feeding rate are measured.

Experiments start with a particle-free fluidization chamber operating at a given fluidization gas flow rate and chimney rotational speed. The solids outlet in one of the end plates of the fluidization chamber[12] is closed during the entire experiment, allowing to control more easily the solids loading in the fluidization chamber and to focus on the solids losses via the chimney.

Solids can be fed to the fluidization chamber via a solids inlet tube in one of the end plates of the fluidization chamber. A first step in the solids feeding rate is realized by starting to feed solids at a given constant rate at time $t_0$ ($t_0 = \pm 10$ s in the figures shown) during a well chosen period (Figure 2). The solids feeding rate $S$ ($3.56 \times 10^{-2}$ kg/s) is chosen such that the change in the fluidization chamber solids loading is relatively slow and the tangential acceleration of the particles by the fluidization gas is sufficiently fast. Furthermore, the solids feeding rate is to be higher than the rate of solids losses via the chimney over a broad range of solids loadings, fluidization gas flow rates, and chimney rotational speeds. The solids feeding period is chosen such ($\Delta t = 70$ s, 2.478 kg solids fed) that the theoretical maximum possible solids loading in the fluidization chamber can be approached, accounting for some solids losses via the chimney, and that the rate of solids losses via the chimney can approach the solids feeding rate. The theoretical maximum solids loading in the fluidization chamber, determined by the particle characteristics and the geometrical dimensions of the fluidization chamber, can be calculated to be

$$\pi \cdot \lfloor (R^{\text{outer}}_{\text{fluid.chamber}})^2 - (R_{\text{chimney}})^2 \rfloor \cdot (L_{\text{fluid.chamber}}) \cdot (\varepsilon^{\text{max}}_{\text{s}}) \cdot (\rho_{\text{s}}) \approx 1.9 \text{ kg}, \quad (4)$$

with $\varepsilon^{\text{max}}_{\text{s}}$ the maximum possible solids volume fraction.

A second step in the solids feeding rate is realized by stopping the solids feeding ($t = \pm 80$ s in the figures) (Figure 2). As, by the action of the rotating chimney, the solids losses via the chimney are limited, after the second step in the solids feeding rate, the change in the fluidization chamber solids loading is assumed to be sufficiently slow for the rotating particle bed to operate under quasi steady-state conditions, that is, the typical time scale of the change in solids loading is expected to be larger than the relaxation time of the rotating particle bed. This was confirmed by the experimental measurements at different chimney rotational speeds. As such, the use of the above described dynamic method allows obtaining experimental data over the entire solids loading range from one single experiment. About 2500 reliable experimental data points were obtained from 12 experiments and 13 repetitive experiments. Furthermore, comparison of the experimental data obtained during and after solids feeding provides some information on the effect of the acceleration of freshly fed particles by the fluidization gas on the pressure drop over the fluidization chamber and on the solids losses via the chimney.

After both step changes in the solids feeding rate, the step responses of the rate of solids losses via the chimney and of the pressure drop over the fluidization chamber are to be

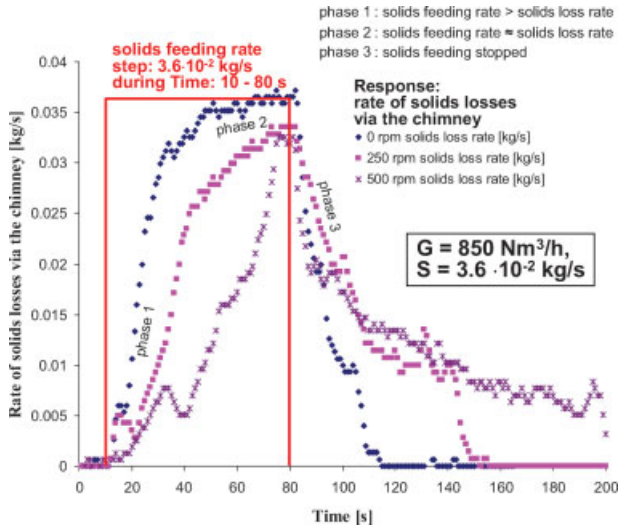


**Figure 2. Dual step response technique.**

Steps in the solids feeding rate given (red curve) and responses in the rate of solids losses via the chimney measured. Illustration with the rates of solids losses via the chimney at a fluidization gas flow rate $G$ of 850 $Nm^3/h$ and a solids feeding rate $S$ of $3.6 \times 10^{-2}$ kg/s, at chimney rotational speeds of 0, 250, and 500 rpm, respectively. Fluidization chamber and particle characteristics: see Table 1. [Color figure can be viewed in the online issue, which is available at www.interscience.wiley.com.]

measured accurately in time. The time interval between two consecutive measurement points is 1 s and is about two orders of magnitude smaller than the system response time, allowing to measure the step response curves with sufficient accuracy. After each experiment, the particle mass balance was verified by stopping the chimney rotational motion and collecting all particles from the fluidization chamber.

The fluidization chamber is 11.5-cm long and has a diameter of 24 cm. The rotating chimney consists of 32 blades and is 7.5-cm long and has a diameter of 16 cm. At its ends, the rotating chimney is closed on one side, i.e. on the side of the motor, opposite the chimney outlet to the cyclone. To prevent significant solids entrainment with the fluidization gas to the chimney via the open end of the rotating chimney, the connection tube between the chimney and the cyclone is extended and enters the chimney to about half of its length. Observations, however, show that, by the action of the centrifugal force, particles entrained with the fluidization gas to the chimney via the open end of the rotating chimney can be returned to the rotating particle bed via the openings in between the blades of the rotating chimney. This is an important second mechanism by which a rotating chimney can reduce (net) solids losses via the chimney (Figure 1b). It should be stressed that the rotating chimney design can be further optimized.

As in rotating fluidized beds in a static geometry,[12,13] the tangential fluidization and the rotational motion of the particle bed against the outer cylindrical wall of the fluidization chamber is obtained by the tangential injection of the fluidization gas via multiple (24) gas inlet slots in the outer cylindrical wall of the fluidization chamber (Figure 1a).[12] Radial fluidization of the particle bed is or can be introduced by forcing the fluidization gas to leave the fluidization chamber via the centrally positioned chimney. The fluidization gas flow rate $G$ is controlled by a mass flow controller and can be varied between 0 and 850 $Nm^3/h$ (0–0.24 $Nm^3/s$). With the fluidization chamber design and particles used in the present work, a minimum fluidization gas flow rate of 650 $Nm^3/h$ is, however, required to be able to overcome gravity and fluidize the particles tangentially, i.e. to obtain a stable rotating particle bed. The chimney rotational speed $\omega_{chimney}$ is controlled by a motor and can be varied between 0 and 2800 rpm. Hence, the chimney rotational speed can be up to about one order of magnitude higher than the typical particle bed rotational speed. In the present work, the chimney rotational speed is varied between 0 and 1500 rpm to cover conditions in which the chimney rotational speed is such that the rotational speed of particles at contact with the chimney is respectively lower, close to, and higher than the average particle bed rotational speed.

Particles can be fed continuously to the fluidization chamber. The solids feeding rate is controlled by a calibrated screw feeder and a sealing rotary valve and can be varied between 0 and $6 \times 10^{-2}$ kg/s.

The present work focuses on the behavior with 1G-Geldart D-type particles. The polymer particles used are cylindrical pellets with a diameter of 5 mm and a length of 2 mm and have a density of 950 $kg/m^3$. The fluidization chamber design and particle characteristics are summarized in Table 1.

## Experimental Results and Discussion

### *Influence of the chimney rotational speed*

Figure 3a shows, for a given fluidization gas flow rate $G$ of 850 Nm3/h and solids feeding rate $S$ of $3.56 \times 10^{-2}$ kg/s, the cumulative solids losses via the chimney as a function of time at different chimney rotational speeds. In each experiment, three distinct phases can be distinguished.

In phase 1 of an experiment (Figure 3b), solids are fed continuously to the fluidization chamber at the given constant

**Table 1. Fluidization Chamber, Rotating Chimney, and Particle Characteristics**

| | Unit | Value |
|---|---|---|
| Fluidization chamber diameter | m | $24 \times 10^{-2}$ |
| Fluidization chamber length | m | $11.5 \times 10^{-2}$ |
| Chimney diameter | m | $16 \times 10^{-2}$ |
| Number of tangential gas inlet slots | | 24 |
| Gas inlet slot width | m | $2.3 \times 10^{-3}$ |
| Number of chimney outlet slots | | 32 |
| Chimney rotational speed | rpm | 0–1,500 |
| Number of solids inlets | | 1, via end plate |
| Total gas flow rate | $Nm^3/h$ | 650–850 |
| Outlet pressure | Pa | 101,300 |
| Temperature | K | 338 |
| Particle material | | polymer |
| Average particle size | m | $2 \times 10^{-3}$ (length) $-5 \times 10^{-3}$ (diameter) (cylinder pellets) |
| Particle density | $kg/m^{-3}$ | 950 |

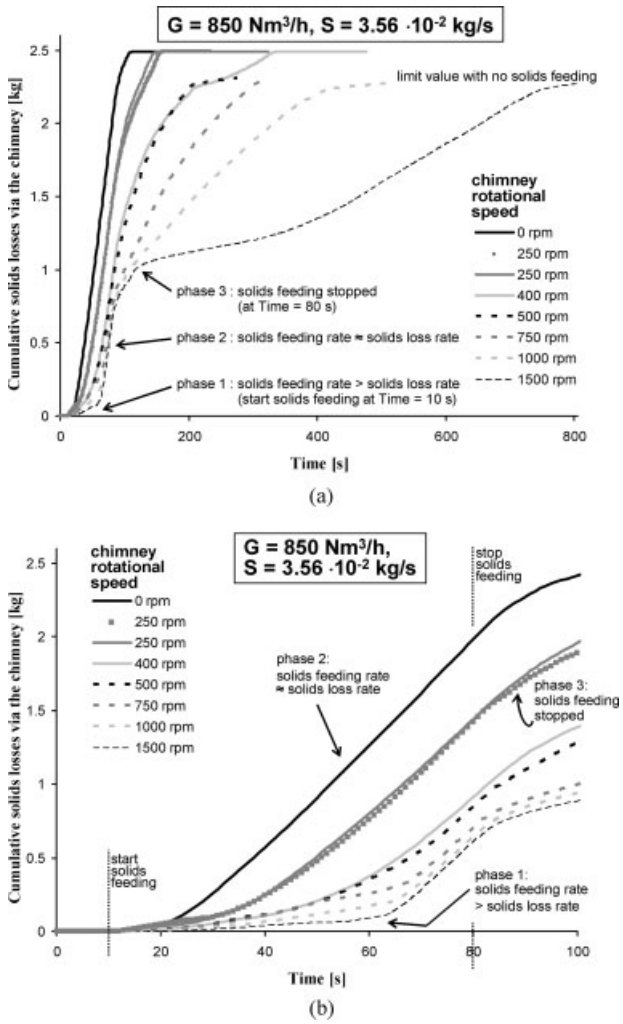


**Figure 3. Cumulative solids losses via the chimney vs. time curves at a fluidization gas flow rate *G* of 850 Nm³/h and a solids feeding rate *S* of 3.56 × 10⁻² kg/s and for varying chimney rotational speed.**

(a) Definition of the different phases; (b) Focus on the first 100 s of the experiments. Fluidization chamber and particle characteristics: see Table 1.

rate and the solids loading in the fluidization chamber is lower than the quasi steady state solids loading. The rate of solids losses via the chimney being smaller than the solids feeding rate, the solids loading in the fluidization chamber is building up. In phase 1, two important characteristics that depend on the chimney rotational speed can be observed: (i) the rate of solids losses via the chimney (Figures 4 and 5b)—affecting the rate at which the solids loading in the fluidization chamber is building up and corresponding to the slope of the cumulative solids losses via the chimney vs. time curves in phase 1 (Figure 3b); (ii) the quasi steady state solids loading in the fluidization chamber that can be reached when feeding solids at the given rate *S* (Figures 5a, b and 6), which corresponds to the solids loading at which the rate of solids losses via the chimney approaches the solids feeding rate (Figures 2 and 5b). Indeed, as will be discussed in more detail further in this paragraph, the rate of solids losses via the chimney increases with increasing solids loading in the fluidization chamber up to the point where the rate of solids losses via the chimney compensates the given solids feeding rate. The dependence of the quasi steady state solids loading on the fluidization gas flow rate is discussed in the next paragraph. Approaching the quasi steady state solids loading corresponds to the onset of phase 2 of an experiment.

The average rate of solids losses via the chimney during phase 1 is shown in Figure 4. As can be seen from Figures 2, 3b, 4, and 5b, in phase 1, the rate of solids losses via the chimney decreases with increasing chimney rotational speed, proving the concept of the rotating chimney.

Figure 5a shows the evolution of the solids loading in the fluidization chamber with time at different chimney rotational speeds. As long as the solids feeding rate is significantly larger than the rate of solids losses via the chimney, the curves at different chimney rotational speeds logically nearly coincide. Figures 5a, b show that the quasi steady state solids loading at given fluidization gas flow and solids feeding rates increases with increasing chimney rotational speed up to the point where the quasi steady state solids loading approaches the theoretical maximum solids loading, determined by the geometry of the fluidization chamber and the chimney (≈1.9 kg).

From the above, it follows that the relation between the chimney rotational speed and the position of the transition point between phase 1 and phase 2 in the cumulative solids losses vs. time curves at given fluidization gas flow and solids feeding rates (Figure 3b) is not straightforward. In fact, this position is influenced by both the above discussed characteristics. The reduction of the rate of solids losses via the chimney with increasing chimney rotational speed allows to build up more rapidly the solids loading in the fluidization chamber. Increasing chimney rotational speeds allow, how-

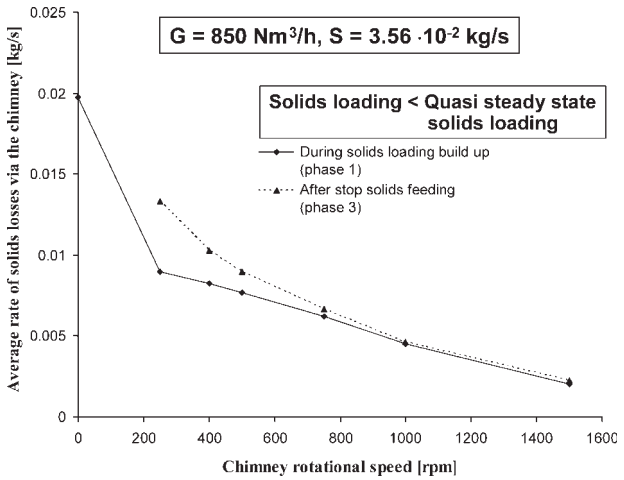


**Figure 4. Average rate of solids losses via the chimney as a function of the chimney rotational speed at solids loadings below the quasi steady state solids loading for the given fluidization gas flow rate *G* of 850 Nm³/h and solids feeding rate *S* of 3.56 × 10⁻² kg/s.**

Fluidization chamber and particle characteristics: see Table 1.

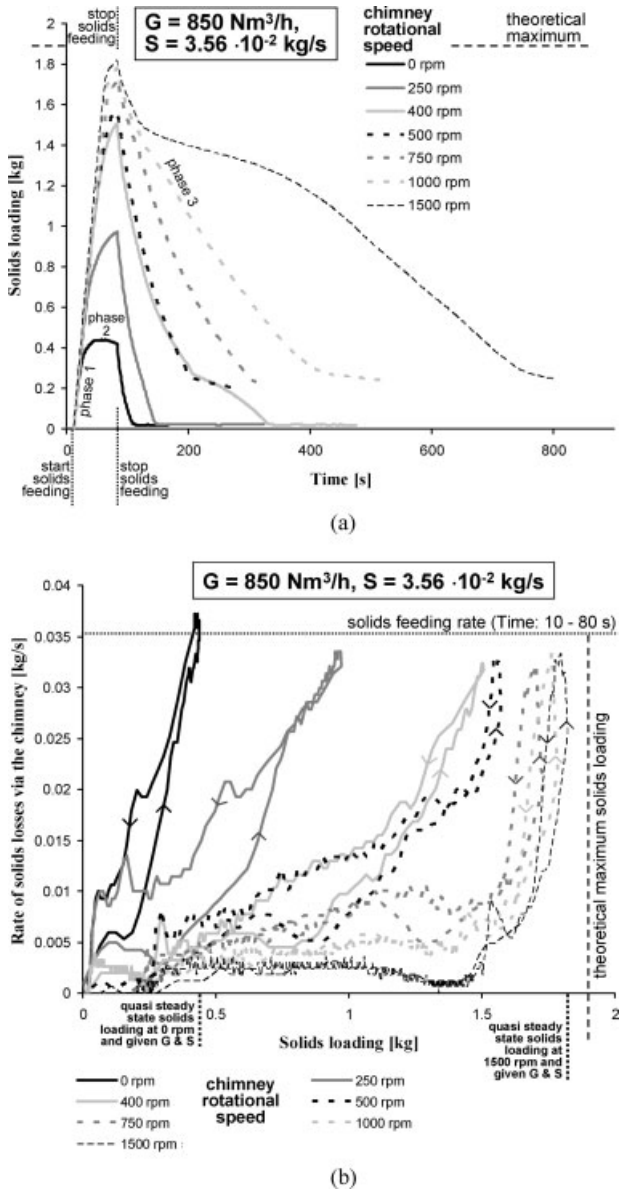


**Figure 5. (a) Solids loading vs. time curves; (b) rate of solids losses via the chimney vs. solids loading curves.**

Fluidization gas flow rate $G$ of 850 $Nm^3/h$ and solids feeding rate $S$ of $3.56 \times 10^{-2}$ kg/s. Varying chimney rotational speed. Fluidization chamber and particle characteristics: see Table 1.

ever, also building up a higher quasi steady state or maximum solids loading in the fluidization chamber.

In phase 2 of an experiment (Figure 3b), solids are still fed continuously at the given constant rate, but, as mentioned above, a quasi steady state operation is reached in which the rate of solids losses via the chimney approaches the solids feeding rate and the solids loading in the fluidization chamber approaches its maximum value for given chimney rotational speed and fluidization gas and solids feeding rates. The increase of the quasi steady state or maximum solids loading at given fluidization gas flow and solids feeding rates with increasing chimney rotational speed is clearly illustrated in Figure 6, showing pictures of the fluidization chamber at the quasi steady state solids loading with a fluidization gas flow rate of 850 $Nm^3/h$ and a solids feeding rate of $3.56 \times 10^{-2}$ kg/s at chimney rotational speeds of respectively 250, 500, and 1000 rpm. For a static chimney (rotational speed = 0), for example, the quasi steady state solids loading in the fluidization chamber at a fluidization gas flow rate of 850 $Nm^3/h$ and a solids feeding rate of $3.56 \times 10^{-2}$ kg/s is only about 0.4 kg (Figures 5a, b), phase 2 starting almost immediately. Phase 2 being characterized by the solids losses via the chimney close to compensating the solids feeding, the slopes of the cumulative solids losses vs. time curves at different chimney rotational speeds (Figures 3a, b) become nearly equal and are exclusively determined by the solids feeding rate.

In phase 3 of an experiment, the solids feeding is stopped (Figures 2 and 3). When the solids feeding is stopped, solids losses via the chimney cause the solids loading in the fluidization chamber to gradually decrease until a new limit value is reached, i.e. the solids loading in the fluidization chamber that remains after stopping the solids feeding, which corresponds to the maximum solids loading with zero solids losses via the chimney. With a static chimney, i.e. at zero chimney rotational speed, the solids losses via the chimney quite rapidly drop when stopping the solids feeding (Figures 2, 3a, and 5a, b), due to the low quasi steady state solids loading in the fluidization chamber that was reached during solids feeding. As the chimney rotational speed increases, the decrease of the solids losses via the chimney and the decrease of the rate of solids losses via the chimney are more gradual (Figures 2, 3a, and 5a, b). Furthermore, as the chimney rotational speed increases, the cumulative solids losses via the chimney from the moment of stopping the solids feeding on decrease (Figure 3a). Hence, the higher the chimney rotational speed, the higher the maximum solids loading with zero solids losses via the chimney.

Figure 5b shows the relation between the rate of solids losses via the chimney and the solids loading in the fluidization chamber at different chimney rotational speeds and for a given fluidization gas flow rate. The arrows in Figure 5b indicate the evolution in time, i.e. from the start to the end of each experiment, allowing to make a distinction between the data on different phases in an experiment (phases as defined in Figures 2, 3, and 5a). The difference between the different phases in Figure 5b is discussed somewhat further in this article. Figures 3b and 5b show that, as long as the solids loading is below the theoretical maximum solids loading, the rate of solids losses via the chimney at a given solids loading in the fluidization chamber decreases with increasing chimney rotational speed. Figure 5b furthermore shows that, the higher the chimney rotational speed, the less the rate of solids losses via the chimney depends on the solids loading in the fluidization chamber, at least for solids loadings below the theoretical maximum. Indeed, the relation between the rate of solids losses via the chimney and the solids loading in the fluidization chamber changes drastically as the theoretical maximum solids loading is approached, the rate of solids losses via the chimney increasing sharply with increasing solids loading and approaching the solids feeding rate (Figures 2 and 5b). To be able to approach the theoretical maximum

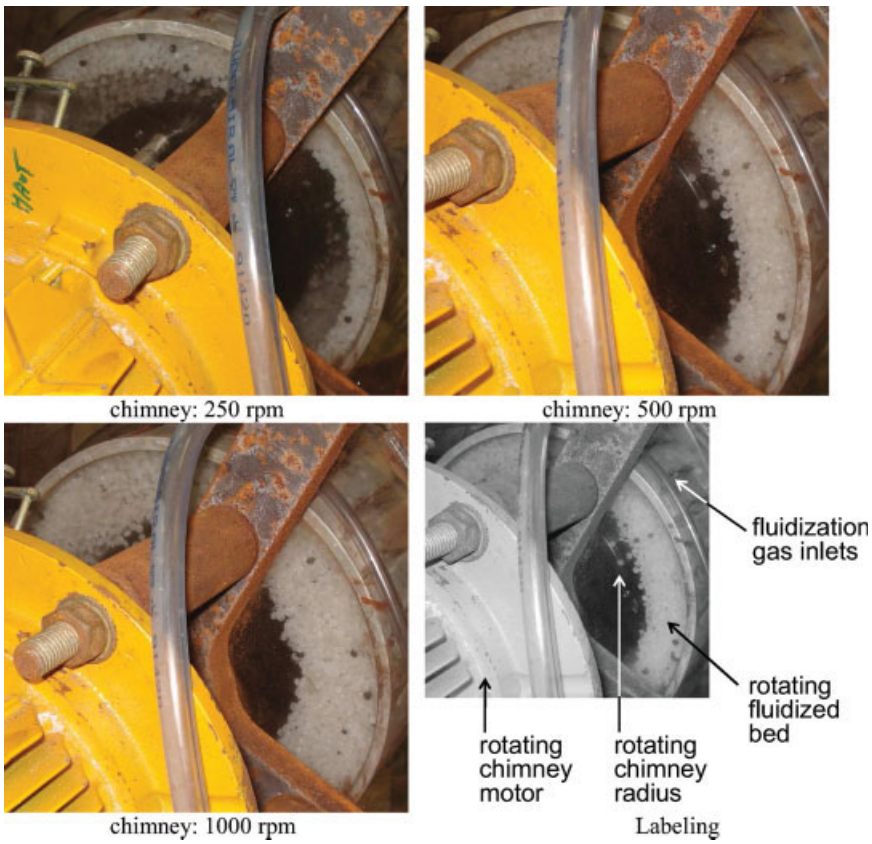


**Figure 6. Pictures of the rotating fluidized bed at the quasi steady state solids loading obtained with different chimney rotational speeds for the given fluidization gas flow rate *G* of 850 Nm$^3$/h and solids feeding rate *S* of 3.56 × 10$^{-2}$ kg/s.**

Average particle bed rotational speed at the quasi steady state solids loading obtained with a chimney rotational speed of 1000 rpm (±1.8 kg): 305 rpm (see Figure 9b). Fluidization chamber and particle characteristics: see Table 1. [Color figure can be viewed in the online issue, which is available at www.interscience.wiley.com.]

solids loading seems to require chimney rotational speeds such that the rotational speed of particles at contact with the chimney is larger than the average particle bed rotational speed (Figures 5a, b), which amounts to a chimney rotational speed of about 750 rpm in the case studied when assuming a particle-chimney slip factor of 0.4 (Figure 9, discussed later in this work). It should be remarked that the average particle bed rotational speed is observed to be hardly influenced by the chimney rotational speed, the direct influence of the rotating chimney being limited to its immediate vicinity.

At solids loadings below the theoretical maximum solids loading and in the absence of solids feeding and acceleration effects (phase 3), the rate of solids losses via the chimney is nearly proportional with the solids loading in the fluidization chamber and inversely proportional with the square of the chimney rotational speed $\omega_{\text{chimney}}$. Hence:

$$[\text{Rate of solids losses via the chimney}] = K \cdot [\text{Solids loading}] \cdot \omega_{\text{chimney}}^{-2}, \qquad (5)$$

with $K = 2800$ in the case studied (Figure 5b).

Figure 7 shows the simulated rate of solids losses via the chimney vs. solids loading curves at different chimney rota-

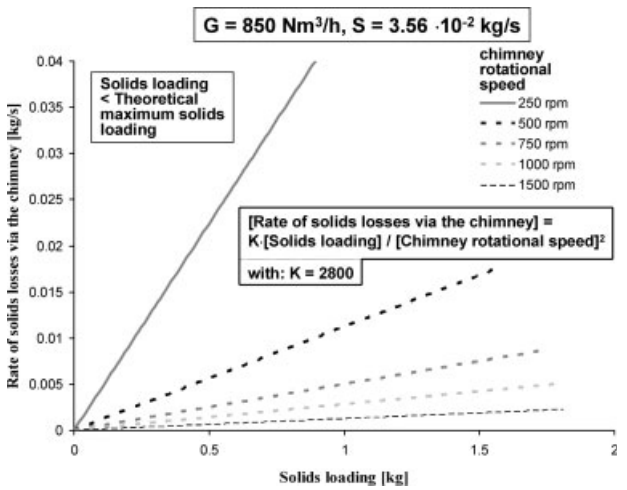


**Figure 7. Simulated rate of solids losses via the chimney vs. solids loading curves for solids loadings below the theoretical maximum solids loading.**

Fluidization gas flow rate *G* of 850 Nm$^3$/h and solids feeding rate *S* of 3.56 × 10$^{-2}$ kg/s. Varying chimney rotational speed. Fluidization chamber and particle characteristics: see Table 1. Experimentally measured behavior: see Figure 5b.

tional speeds for solids loadings below the theoretical maximum (phases 1 and 3) using Eq. 5. Comparing Figures 5 and 7 shows that Eq. 5 predicts the relation between the rate of solids losses via the chimney, the solids loading in the fluidization chamber and the chimney rotational speed for solids loadings below the theoretical maximum with reasonable accuracy. As the centrifugal force generated by the rotating chimney is proportional to the square of the chimney rotational speed, Eq. 5 learns that the rate of solids losses via the chimney is inversely proportional with the centrifugal force by the rotating chimney $F_c^{\text{chimney}}$:

$$[\text{Rate of solids losses via the chimney}] = \tilde{K} \cdot [\text{Solids loading}] \cdot [F_c^{\text{chimney}}]^{-1}. \quad (6)$$

The relation between the proportionality constant $\tilde{K}$ in Eq. 6 and the geometrical characteristics of the chimney is to be further investigated.

It should be remarked that at lower chimney rotational speeds, that is chimney rotational speeds such that the rotational speed of particles at contact with the chimney is below the average particle bed rotational speed, the solids feeding and acceleration affects to a certain extent the relation between the rate of solids losses via the chimney and the solids loading, at least at lower solids loadings (Figures 4 and 5b). Somewhat surprisingly, for a given solids loading, the rate of solids losses via the chimney is lower during solids feeding (phase 1, arrows pointing upwards in Figure 5b) than during solids discharge, i.e. after stopping the solids feeding (phase 3, arrows pointing downwards in Figure 5b). This may be due to the way the particles are fed to the fluidization chamber.[12] The solids inlet is located in the end plate of the fluidization chamber at the side of the open chimney end (Figure 1b) and the particles are, hence, blown into the fluidization chamber toward the opposite side, that is, the side of the closed chimney end (Figure 1b). Particles are expected to be mainly entrained into the chimney via its open end. At solids loadings below the theoretical maximum solids loading, particles entrained to the chimney via its open end are returned to the particle bed at relatively high chimney rotational speeds (see previous paragraph and Figure 1b), but not at relatively low chimney rotational speeds. In the latter case, somewhat lower solids losses via the chimney may be observed during initial solids feeding.

A practical interpretation of Figure 5b is that, to maintain a given solids loading in the fluidization chamber, the solids feeding rate required to compensate for solids losses via the chimney decreases with increasing chimney rotational speed. As such and to a certain extent, the chimney rotational speed can be used to control the particle residence time in the fluidization chamber. This interesting feature of the rotating chimney is demonstrated in Figure 8, showing the average particle residence time in the fluidization chamber as a function of the chimney rotational speed for a solids loading of 1 kg and a fluidization gas flow rate of 850 $Nm^3$/h. As expected from Eq. 5, a more than proportional increase of the average solids residence time in the fluidization chamber with increasing chimney rotational speed is experimentally observed.

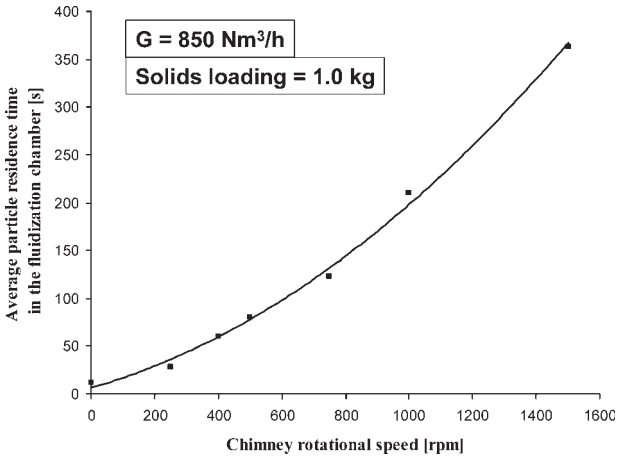


**Figure 8. Experimentally measured average particle residence time in the fluidization chamber as a function of the chimney rotational speed for a solids loading of 1 kg in the fluidization chamber and a fluidization gas flow rate *G* of 850 $Nm^3$/h.**

Fluidization chamber and particle characteristics: see Table 1.

Figure 5b most clearly illustrates the advantages of using a rotating chimney for rotating fluidized beds. At given fluidization gas flow and solids feeding rates, sufficiently high chimney rotational speeds allow to increase the solids loading in the fluidization chamber up to the theoretical maximum (Figures 5a, b). Furthermore, at sufficiently high chimney rotational speeds, the rate of solids losses via the chimney is drastically reduced and becomes almost independent of the solids loading in the fluidization chamber over a broad solids loading range (Figure 5b).

Figure 9a shows an illustrative example of the relation between the fluidization gas flow rate and the radial drag force and centrifugal force in the rotating particle bed generated by the fluidization gas in the vicinity of the chimney, as well as the relation between the chimney rotational speed and the centrifugal force exerted by the rotating chimney on the particles at contact with the chimney. Based on the experimental observations (Figure 6), the solids volume fraction in the particle bed is assumed to be 0.6 in Figure 9. The radial drag force per cubic meter particle bed can then be calculated from[15]:

$$F_{\text{drag}}^{\text{rad}} = \beta(u_r - v_r) \approx \beta u_r, \quad (7)$$

the drag coefficient $\beta$ being given by[15]:

$$\beta = 150\frac{\varepsilon_s^2}{\varepsilon_g}\frac{\mu_g}{(d_p\phi)^2} + 1.75\frac{\varepsilon_s\rho_g}{d_p\phi}|\overline{u} - \overline{v}|. \quad (8)$$

In Eq. 7, the radial solids velocity $v_r$ is assumed to be negligible, in accordance with the experimental observations, whereas the interstitial radial gas phase velocity $u_r$ can be calculated from the fluidization gas flow rate $G$, the dimen-

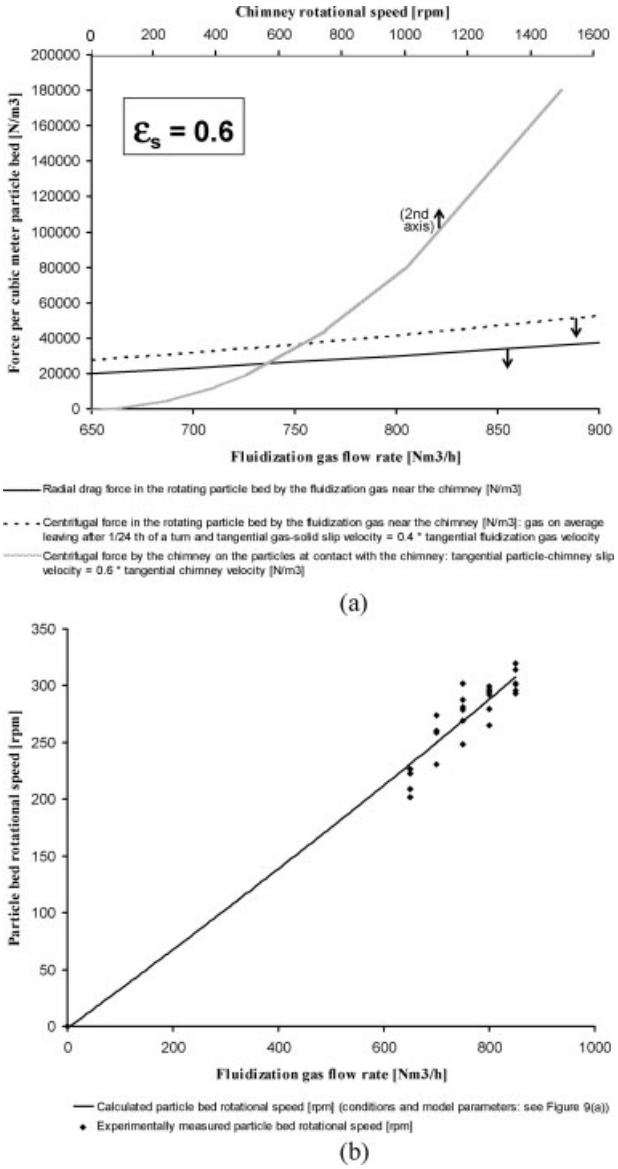


**Figure 9. (a) Illustrative example of the radial drag and centrifugal forces generated by the fluidization gas in the rotating particle bed in the vicinity of the chimney as a function of the fluidization gas flow rate and of the centrifugal force generated by the rotating chimney on the particles at contact with the chimney as a function of the chimney rotational speed (Eqs. 7–10); (b) experimentally measured and calculated particle bed rotational speeds at the quasi steady state solids loading (±1.8 kg, see Figures 13 and 14) with a solids feeding rate *S* of 3.56 × $10^{-2}$ kg/s and a chimney rotational speed of 1000 rpm.**

(a and b) Fluidization chamber and particle characteristics: see Table 1. Model assumptions: $\varepsilon_s = 0.6$, $v_{rad} = 0$, $\langle n_g^{rotations} \rangle = 1/24$, $s_{tan\,g}^{gs} = 0.6$, and $s_{tan\,g}^{sc} = 0.4$.

sions of the fluidization chamber, the particle bed solids volume fraction, and the radial position in the fluidization chamber.[12]

Using Eqs. 1–3 and assuming a solid body rotation type motion of the rotating particle bed, the centrifugal force per cubic meter particle bed near the chimney generated by the fluidization gas can be estimated from:

$$F_c^{bed/chimney} = \langle \tilde{\omega}_{bed} \rangle^2 \cdot R_{chimney} \cdot \varepsilon_s \cdot \rho_s, \tag{9}$$

where the influence of the rotational motion of the chimney on the average particle bed rotational speed can be neglected, as experimentally observed. In Figure 9, the fluidization gas is assumed to leave the fluidization chamber after an average 15° rotation, corresponding to $\langle n_g^{rotations} \rangle = 360° \cdot [\text{Number of tangential gas inlet slots}]^{-1}$ (Eq. 3 and Table 1), and the tangential gas–solid slip factor in the rotating particle bed $s_{tan\,g}^{gs}$ (Eq. 3) is assumed to be 0.6, independent of the fluidization gas flow rate. The constant values of $\langle n_g^{rotations} \rangle$ and $s_{tan\,g}^{gs}$ over a certain fluidization gas flow rate range are experimentally demonstrated in Figure 9b, showing experimentally measured particle bed rotational speeds as a function of the fluidization gas flow rate at the quasi steady state solids loading (±1.8 kg, see Figures 13 and 14) at a chimney rotational speed of 1000 rpm. As mentioned before, the chimney rotational speed has only a limited impact on the average particle bed rotational speed measured.

The particle bed rotational speed is seen to increase proportionally with the fluidization gas flow rate, allowing to assume values of $\langle n_g^{rotations} \rangle$ and $s_{tan\,g}^{gs}$ independent of the fluidization gas flow rate. Figure 9b furthermore shows that, with the given model parameters, model Eqs. 1–3 allow to predict quite accurately the experimentally observed particle bed rotational speeds. For the given solids loading, the latter vary roughly between 200 and 300 rpm for fluidization gas flow rates between 650 and 850 $Nm^3/h$.

The centrifugal force by the rotating chimney on the particles at contact with the chimney and per cubic meter particle bed, also shown in Figure 9, can be calculated from:

$$F_c^{chimney} = \tilde{\omega}_{chimney}^2 \cdot R_{chimney} \cdot \varepsilon_s \cdot \rho_s \cdot (s_{tan\,g}^{sc})^2, \tag{10}$$

where $s_{tan\,g}^{sc}$ is the previously introduced tangential particle-chimney slip factor. The tangential particle-chimney slip factor is expected to depend on the shape of the chimney blades, the chimney material, the type of particles, and most probably the chimney rotational speed. An expression for the tangential particle-chimney slip factor requires further investigations and a constant value of 0.4 is assumed in Figure 9.

Accounting for its assumptions, Figure 9a indicates that with the current fluidization chamber design and for the 1G-Geldart D-type particles used, radial fluidization by the fluidization gas is hardly possible. This is confirmed by the visual observations (Figure 6) and the pressure drop measurements discussed further in this work. The fluidization chamber is behaving like a strongly vibrating moving belt, supporting the particle bed (because of the high centrifugal force) crossed by the gas flow. The vibrating motion is due to the periodical (in space) injection of the fluidization gas in the fluidization chamber and results in good radial mixing of the particles in the rotating particle bed. Figure 9 nicely illustrates the similar increase of the radial gas–solid drag force and the centrifugal force in the rotating particle bed with

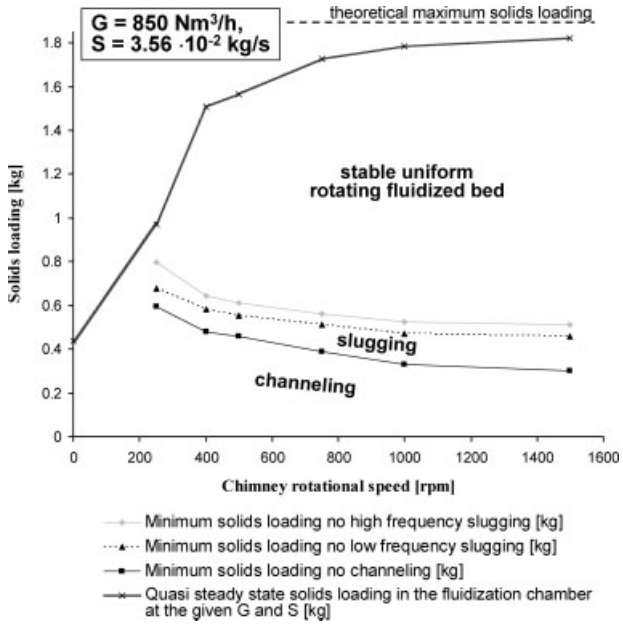


**Figure 10. Quasi steady state solids loading in the fluidization chamber as a function of the chimney rotational speed, and the different flow regimes (channeling, slugging, stable rotating fluidized bed) as a function of the chimney rotational speed and the solids loading in the fluidization chamber.**

Fluidization gas flow rate $G$ of 850 $Nm^3/h$ and solids feeding rate $S$ of $3.56 \times 10^{-2}$ kg/s. Fluidization chamber and particle characteristics: see Table 1.

increasing fluidization gas flow rate. The centrifugal force being somewhat more strongly affected by the fluidization gas flow rate than the radial gas–solid drag force (Figure 9a), a radial bed contraction, rather than a radial bed expansion is expected with increasing fluidization gas flow rate. As described by De Wilde and de Broqueville,[12] this is a major advantage of this type of rotating fluidized beds, offering increased flexibility with respect to the fluidization gas flow rate. The influence of the fluidization gas flow rate is discussed in detail in the next paragraph.

During the dynamic experiments, the conditions at which the different flow regimes (i.e. channeling, slugging, and a stable rotating fluidized bed) occur were monitored. As described in De Wilde and de Broqueville,[12] channeling is a steady, longitudinally nonuniform distribution of the particles in the fluidization chamber, whereas slugging is a dynamic, quasi-steady, tangentially nonuniform distribution of the particles in the fluidization chamber. Figure 10 shows for a fluidization gas flow rate $G$ of 850 $Nm^3/h$, the different flow regimes as a function of the solids loading and the chimney rotational speed. The dependence of the flow regime on the fluidization gas flow rate is shown in Figure 14, discussed in the next paragraph. The flow regime is observed to mainly depend on the solids loading in the fluidization chamber, confirming the limited direct influence of the chimney rotational motion on the average rotating fluidized bed behavior (average particle bed rotational speed,...). In fact, the rotating chimney mainly allows reducing the solids losses via the chimney, increasing the solids residence time in the fluidization chamber at given solids loading and fluidization gas flow rate, and increasing the solids loading in the fluidization chamber at given fluidization gas flow and solids feeding rates, and in this way indirectly affects the overall or average rotating fluidized bed behavior and the operating conditions required to achieve the different flow regimes mapped in Figure 10. As seen from Figure 10, channeling is observed at the lowest solids loadings. At somewhat higher solids loadings, low and high frequency slugging occur. Over a broad solids loading range, however, that is, at sufficiently high solids loadings, a stable rotating fluidized bed can be obtained. It should be emphasized that higher solids loadings can be achieved more easily, that is, at lower solids feeding rates, as the chimney rotational speed increases.

### *Influence of the fluidization gas flow rate/velocity*

Figures 11a, b show the cumulative solids losses via the chimney vs. time curves at a chimney rotational speed of 1000 rpm and a solids feeding rate of $3.56 \times 10^{-2}$ kg/s for different fluidization gas flow rates in the range 650–850 $Nm^3/h$. The relation between the fluidization gas flow rate and the particle bed rotational speed at the quasi steady state solids loading was described in Figure 9b. The relation between the average radial gas velocity, which roughly equals the average radial gas–solid slip velocity, and the fluidization gas flow rate is given in Figure 12 (2nd $x$-axis). For the definition of the different phases during an experiment, reference is made to the previous paragraph where it was also shown that at a chimney rotational speed of 1000 rpm and the given solids feeding rate, the quasi steady state solids loading in the fluidization chamber easily approaches the theoretical maximum. Figure 11b focuses on phase 1 of the experiments, i.e. when the solids loading in the fluidization chamber is building up. A similar behavior in phase 1 and phase 3 of the experiments, i.e. at solids loadings below the theoretical maximum solids loading, is observed. As confirmed by the average rate of solids losses via the chimney vs. fluidization gas flow rate curves (Figure 12) and by the rate of solids losses via the chimney vs. solids loading curves (Figure 13b), at solids loadings below the theoretical maximum solids loading (phases 1 and 3), the rate of solids losses via the chimney slightly decreases with increasing fluidization gas flow rate. A possible explanation for this observation, is that the centrifugal force in the particle bed is somewhat more sensitive to the fluidization gas flow rate than the radial gas–solid drag force. Indeed, in the fluidization gas flow rate range investigated, a linear increase of the particle bed rotational speed with increasing fluidization gas flow rate was measured (Figure 9b). The stronger impact of the fluidization gas flow rate on the centrifugal force than on the radial gas–solid drag force, theoretically demonstrated in Figure 9a and already described by De Wilde and de Broqueville,[12] causes a slight radial bed contraction with increasing fluidization gas flow rate, rather than a radial bed expansion, resulting in the experimentally observed reduction of the solids losses via the chimney with increasing fluidization gas flow rate at solids loadings below the theoretical maximum solids loading. At solids loadings close to the theoretical maximum solids loading (phase 2), however, the particle bed

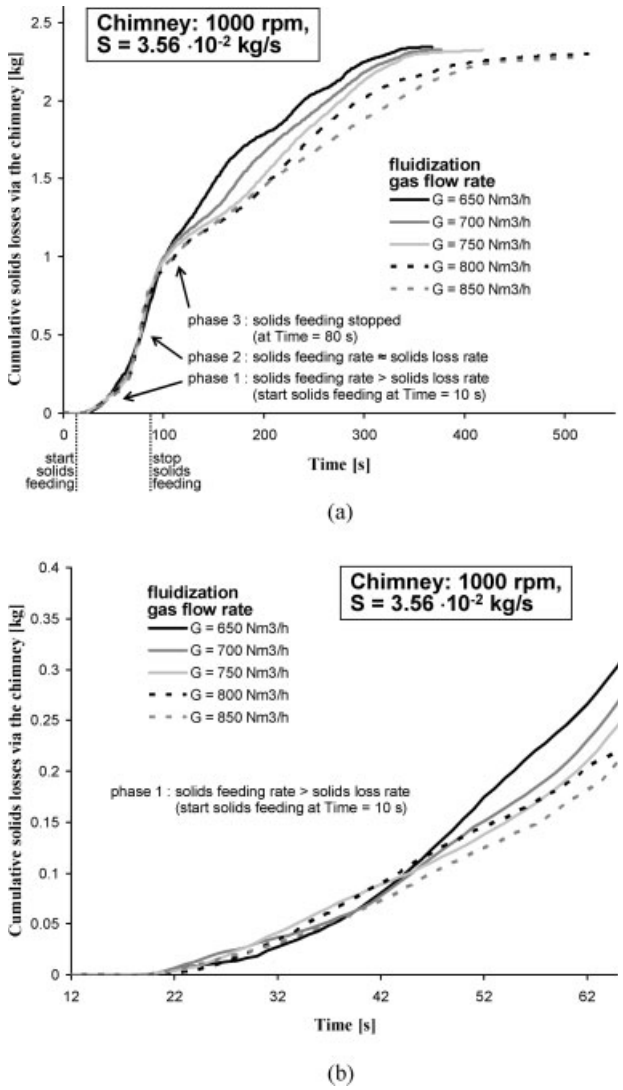


**Figure 11. Cumulative solids losses vs. time curves at a chimney rotational speed of 1000 rpm and a solids feeding rate $S$ of 3.56 × $10^{-2}$ kg/s and for varying fluidization gas flow rates.**

(a) Definition of the different phases; (b) Focus on the first phase of the experiments. Fluidization chamber and particle characteristics: see Table 1.

freeboard approaches the chimney. The smaller the radial distance to the center of the fluidization chamber, the higher the ratio of the radial drag to centrifugal force, for example resulting in the phenomenon of layered fluidization in rotating fluidized beds.[3–7,9] Furthermore, as the solids loading approaches the theoretical maximum, local phenomena, related to particle-chimney interactions, become more important. As a result, at solids loadings approaching the theoretical maximum solids loading (phase 2), the rate of solids losses via the chimney is seen to increase slightly with increasing fluidization gas flow rate (Figure 13b).

Figures 13a, b show that, at given chimney rotational speed and solids feeding rate, the quasi steady state solids loading in the fluidization chamber slightly decreases with increasing fluidization gas flow rate, due to the increased rate of solids losses via the chimney at higher fluidization gas flow rates when the theoretical maximum solids loading is approached.

The different flow regimes as a function of the solids loading and the fluidization gas flow rate are mapped in Figure 14 for a chimney rotational speed of 1000 rpm and a solids feeding rate $S$ of 3.56 × $10^{-2}$ kg/s. Figure 14 also shows the quasi steady state solids loading in the fluidization chamber at the given conditions. The flow regime is seen to depend mainly on the solids loading in the fluidization chamber, the fluidization gas flow rate only having a minor effect. Still, the minimum solids loading required to obtain a stable rotating fluidized bed decreases slightly with increasing fluidization gas flow rate. The dependence of the flow regime on the solids loading is in line with the observations in and the discussion on Figure 10 in the previous paragraph. To maintain a sufficiently high solids loading in the fluidization chamber for a stable uniform rotating fluidized bed operation, the solids feeding rate required to compensate for the solids losses via the chimney depends mainly on the chimney rotational speed (Figure 5b), the solids loading in the fluidization chamber (Figures 5b and 13b) and the fluidization gas flow rate (Figure 13b), and can be made small if required by the application. Alternatively and as mentioned earlier, the rate of solids losses via the chimney could be used to control the particle residence time in the fluidization chamber.

The relation between the pressure drop over the fluidization chamber and the solids loading and the fluidization gas flow rate was measured and is shown in Figures 15a, b for a chimney rotational speed of 1000 rpm. It should be remarked that,

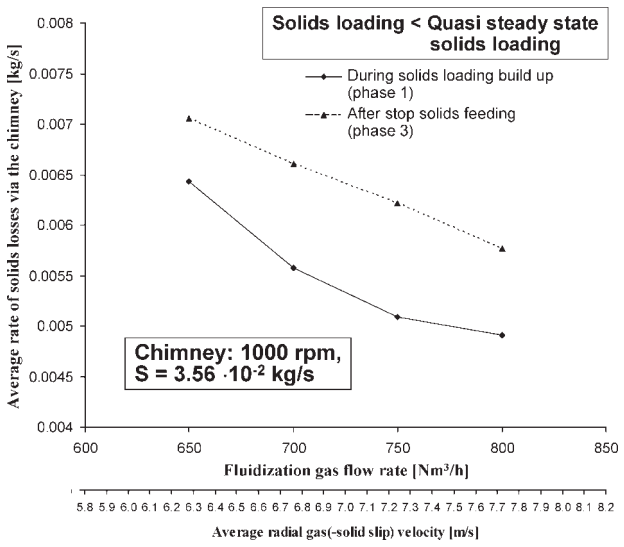


**Figure 12. Average rate of solids losses via the chimney as a function of the fluidization gas flow rate at solids loadings below the quasi steady state solids loading for the given chimney rotational speed of 1000 rpm and solids feeding rate $S$ of 3.56 × $10^{-2}$ kg/s.**

Fluidization chamber and particle characteristics: see Table 1. Second $x$-axis: average radial gas(-solid slip) velocity in the rotating particle bed at a solids volume fraction $\varepsilon_s$ of 0.6 corresponding with the fluidization gas flow rate $G$ shown on the first $x$-axis.

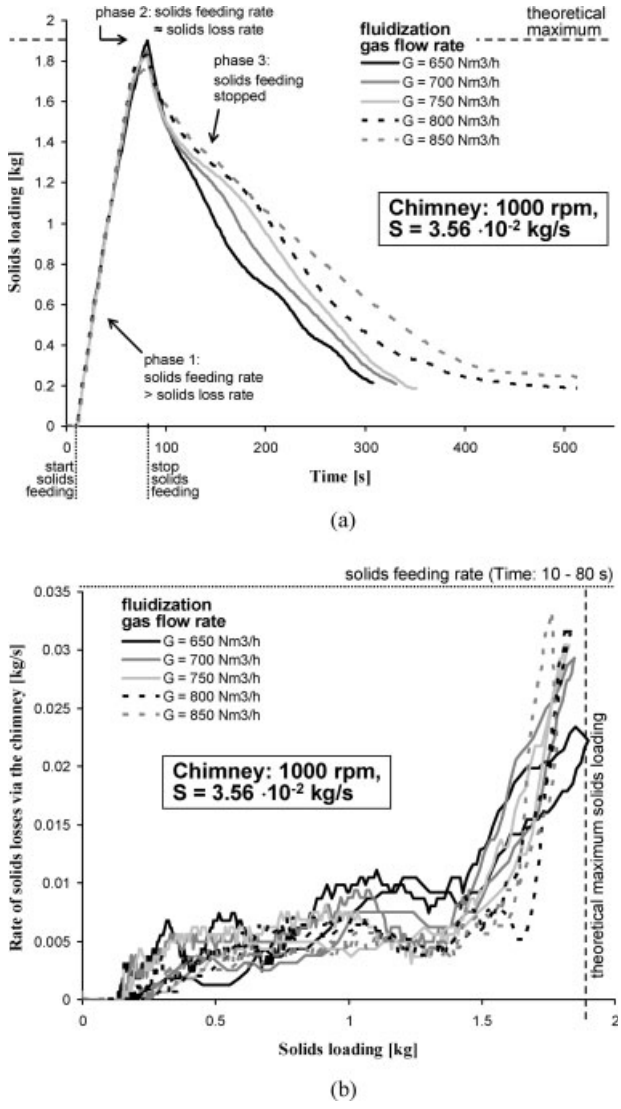


**Figure 13. (a) Solids loading vs. time curves; (b) Rate of solids losses via the chimney vs. solids loading curves.**

Chimney rotational speed of 1000 rpm and solids feeding rate $S$ of $3.56 \times 10^{-2}$ kg/s. Varying fluidization gas flow rate. Fluidization chamber and particle characteristics: see Table 1.

when feeding the first particles to the fluidization chamber, the gas flow behavior drastically changes (Figure 15a), resulting in an initial decrease of the pressure drop over the fluidization chamber when feeding solids. As soon as particles are present in the fluidization chamber, the average gas phase tangential velocity is expected to decrease, the particles acting as deflectors. The reduction of the average tangential gas phase velocity is reflected in the initial pressure drop reduction when feeding particles to the fluidization chamber (Figure 15a). Most probably, in the absence of particles, the fluidization gas is on average making one or multiple rotations in the fluidization chamber before leaving via the chimney, whereas as soon as particles are introduced, the fluidization gas is on average making less than one rotation in the fluidization chamber before leaving via the chimney.[16] It should also be remarked that, under the experimental conditions investigated (Table 1), the main part of the pressure drop over the fluidization chamber is clearly related to the gas phase (Figure 15a) and not to the presence of the particles. Figure 16 shows the pressure drop over the fluidization chamber specifically caused by the solids, that is, the pressure drop over the rotating particle bed, per unit mass solids loading as a function of the gas flow rate. The pressure drop over the fluidization chamber (Figures 15a, b) is defined and measured as the difference between the pressure in the gas distribution chamber surrounding the fluidization chamber and the pressure in the static chimney tube (Figure 1b). The high gas phase contribution to the pressure drop over the fluidization chamber is mainly due to the high velocity injection of the fluidization gas in the fluidization chamber via the narrow tangential gas inlet slots. As shown in Figure 17, the gas phase pressure drop over the fluidization chamber related to the rotational motion of the chimney is at its maximum still about one order of magnitude smaller than the gas phase pressure drop over the fluidization chamber gas inlet slots. For a fluidization gas flow rate of 800 $Nm^3/h$ and a chimney rotational speed of 1000 rpm, for example, the gas phase pressure drop due to the rotational motion of the chimney is about 950 Pa (Figure 17). Remarkably, the gas phase pressure drop due to the rotational motion of the chimney initially decreases with increasing chimney rotational speed and actually becomes negative. This indicates that at very low

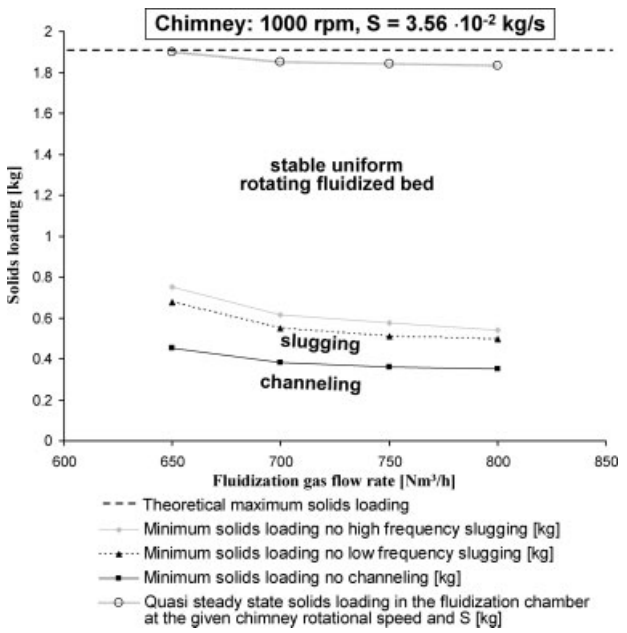


**Figure 14. Quasi steady state solids loading in the fluidization chamber as a function of the fluidization gas flow rate, and the different flow regimes (channeling, slugging, stable rotating fluidized bed) as a function of the fluidization gas flow rate and the solids loading in the fluidization chamber.**

Chimney rotational speed of 1000 rpm and solids feeding rate $S$ of $3.56 \times 10^{-2}$ kg/s. Fluidization chamber and particle characteristics: see Table 1.

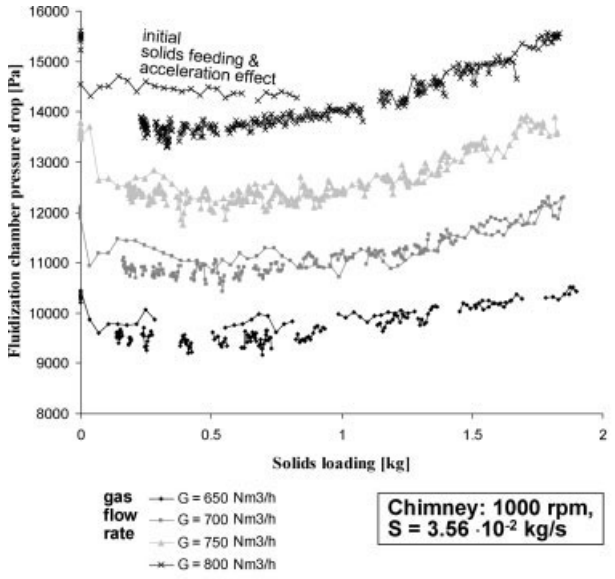


(a)

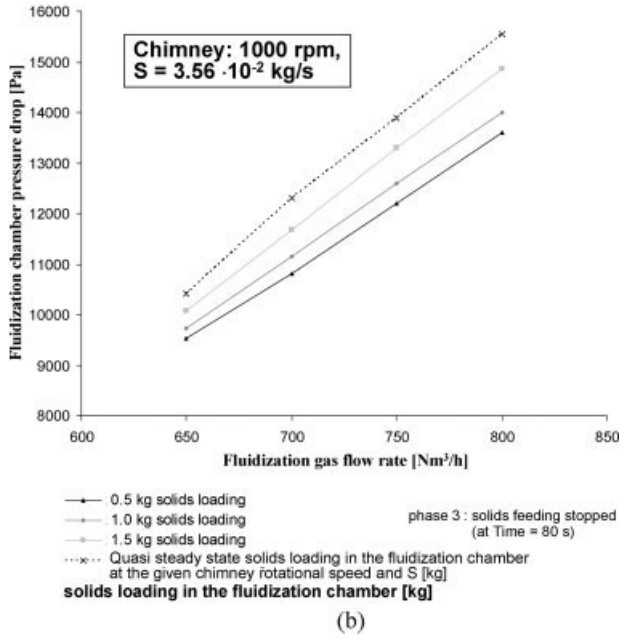


(b)

**Figure 15. (a) Pressure drop over the fluidization chamber as a function of the solids loading for varying fluidization gas flow rates; (b) pressure drop over the fluidization chamber as a function of the fluidization gas flow rate for different solids loadings in the fluidization chamber.**

Fluidization chamber and particle characteristics: see Table 1.

chimney rotational speeds, the rotational motion of the chimney makes it easier for the fluidization gas to move from the fluidization chamber to the chimney. At chimney rotational speeds above 200 rpm, however, the gas phase pressure drop due to the rotational motion of the chimney is seen to increase with increasing chimney rotational speed, the rotating motion

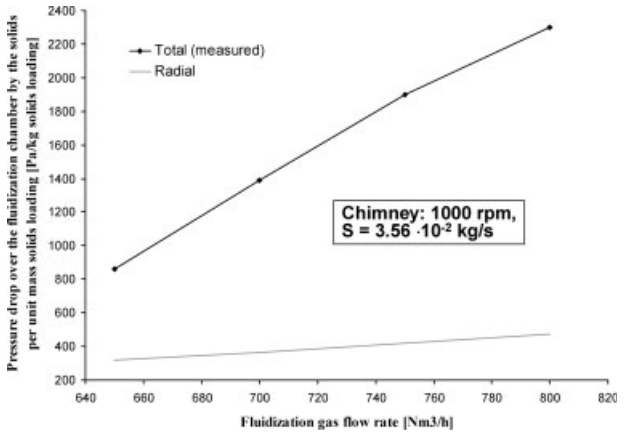


**Figure 16. Pressure drop over the fluidization chamber by the solids, that is, over the rotating particle bed, per unit mass solids loading as a function of the fluidization gas flow rate.**

Stable uniform rotating fluidized bed regime. Experimentally measured total value and radial component shown. Assumptions for the calculation of the radial component: see Figure 9.

of the chimney making it more difficult for the fluidization gas to move from the fluidization chamber to the chimney.

Regarding the solids contribution to the pressure drop over the fluidization chamber, an initial solids feeding and acceleration effect is observed in the pressure drop vs. solids loading curves (Figure 15a). Independent of this effect, at lower solids loadings, that is, at solids loadings where channeling and slugging occur (Figures 10 and 14), the pressure drop over the fluidization chamber is seen to be hardly affected by the solids loading in the fluidization chamber (Figures 15a, b), the fluidization gas bypassing most of the particles in the fluidization chamber. At higher solids loadings, that is, in the stable rotating fluidized bed regime (Figures 10 and 14), the pressure drop over the fluidization chamber is seen to increase nearly propor-

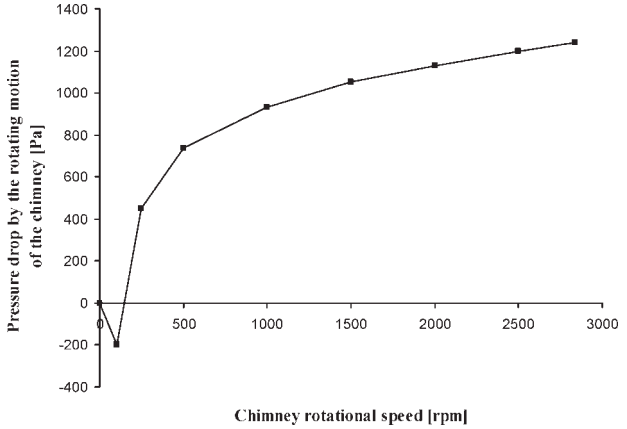


**Figure 17. Experimentally measured contribution of the rotational motion of the chimney to the pressure drop over the fluidization chamber.**

Fluidization gas flow rate of 800 $Nm^3/h$.

tionally with the solids loading in the fluidization chamber (Figures 15a, b). Furthermore, Figures 15a, b learn that the pressure drop over the fluidization chamber increases proportionally with the fluidization gas flow rate $G$, whereas Figure 16 learns that the pressure drop over the fluidization chamber specifically related to the solids, that is, the pressure drop over the rotating particle bed, also increases proportionally with the fluidization gas flow rate $G$. Hence:

$$\Delta P^{\text{fluidization chamber}}_{\text{stable rotating fluidized bed}} = \Delta P^{\text{gas phase}}_{\text{stable rotating fluidized bed}} + \Delta P^{\text{rotating particle bed}}_{\text{stable rotating fluidized bed}} = C_g \cdot G + C_p \cdot G \cdot [\text{Solids loading}]. \quad (11)$$

The pressure drop over the rotating particle bed $\Delta P^{\text{rotating particle bed}}_{\text{stable rotating fluidized bed}}$ can be decomposed into two main contributions:

$$\Delta P^{\text{rotating particle bed}}_{\text{stable rotating fluidized bed}} = \Delta P^{\text{rotating particle bed}^{\text{rad}}}_{\text{stable rotating fluidized bed}} + \Delta P^{\text{rotating particle bed}^{\text{tan g}}}_{\text{stable rotating fluidized bed}}. \quad (12)$$

The first contribution $\Delta P^{\text{rotating particle bed}^{\text{rad}}}_{\text{stable rotating fluidized bed}}$ is related to the radial fluidization of the particle bed, that is, the radial gas–solid drag force. As such, the radial pressure drop contribution $\Delta P^{\text{rotating particle bed}^{\text{rad}}}_{\text{stable rotating fluidized bed}}$ can be estimated from:

$$\Delta P^{\text{rotating particle bed}^{\text{rad}}}_{\text{stable rotating fluidized bed}} = \langle F^{\text{rad}^{\text{bed}}}_{\text{drag}} \rangle \cdot \Delta H^{\text{bed}}, \quad (13)$$

where $\langle F^{\text{rad}^{\text{bed}}}_{\text{drag}} \rangle$ is the average radial gas–solid drag force in the fluidization chamber per cubic meter particle bed. It should be remarked that in case the centrifugal force in the rotating particle bed is larger than the radial gas–solid drag force (Figure 9) and a kind of rotating and vibrating packed bed against the outer cylindrical wall of the fluidization chamber is formed, a force additional to the radial gas–solid drag force is carried out by the outer cylindrical wall of the fluidization chamber to support or carry the rotating particle bed and its weight in the centrifugal field. This effect is not seen in the pressure drop over the fluidization chamber or over the rotating particle bed.

The second contribution to the pressure drop over the rotating particle bed $\Delta P^{\text{rotating particle bed}^{\text{tan g}}}_{\text{stable rotating fluidized bed}}$ is related to the tangential fluidization of the particle bed, that is, the shear resulting from particle–particle and particle-wall collisions.

According to Figures 9 and 16 and using the average fluidization chamber radius in the calculation of the radial gas–solid drag force (Eqs. 7, 8, and 13), for fluidization gas flow rates of respectively 650 and 800 $Nm^3/h$ and for the theoretical maximum solids loading in the fluidization chamber at a solids volume fraction of 0.6, $\Delta P^{\text{rotating particle bed}^{\text{rad}}}_{\text{stable rotating fluidized bed}}$ is respectively only about 600 and 850 Pa (Eq. 13). Comparison with the total pressure drop over the fluidization chamber measured (Figure 15a), i.e. respectively 10,500 and 15,500 Pa at the given conditions, and with the total pressure drop over the rotating particle bed measured (Figure 16), i.e. respectively about 1650 and 4150 Pa at the given conditions, and accounting for the pressure drop contribution of the rotating chimney (Figure 17), learns that respectively about 80 and 65% of the pressure drop over the fluidization chamber is related to the injection of the fluidization gas in the fluidization chamber. Furthermore, the tangential fluidization of the particle bed, i.e. the particle bed rotational motion and the shear resulting from particle–particle and particle-wall collisions, is at the origin of respectively about 60 and 80% of the pressure drop over the rotating particle bed, corresponding to respectively about 10 and 20% of the pressure drop over the fluidization chamber. The high particle density in the rotating particle bed (close to packed bed for the 1G-Geldart D-type particles used) (Figure 6) (Eqs. 7 and 8; Ref. 15), the absence of radial fluidization of the particle bed, and the main contribution of the shear, could explain the linear increase of the pressure drop over the rotating particle bed with the fluidization gas flow rate (Figures 15a, b and 16).

It should be remarked that the centrifugal pressure drop over the fluidization chamber (in the radial direction and resulting from the weight of the particle bed in the centrifugal field) amounts to about 1000 and 2250 Pa, for a fluidization gas flow rate of respectively 650 and 800 $Nm^3/h$, as can be derived from Figure 9. The difference between the centrifugal pressure drop over the fluidization chamber and the radial pressure drop over the fluidization chamber (respectively 600 and 850 Pa, see above) is due to the lack of radial fluidization with the fluidization chamber design and particles used in the present work. As mentioned earlier, this difference is carried by the cylindrical outer wall of the fluidization chamber against which the particles are being pushed.

## Conclusions

The new concept of a rotating chimney for rotating fluidized beds has been experimentally proven and investigated using 1G-Geldart D-type particles. The rotating chimney consists of multiple blades with openings to the chimney in between them and rotates in the same sense as the rotating particle bed, but not necessarily at the same rotational speed. In particular, chimney rotational speeds such that the rotational speed of particles at contact with the chimney is higher than the average particle bed rotational speed are advantageous.

The rotating chimney allows to increase locally, that is, in the vicinity of the chimney, the centrifugal force, preventing the particles from leaving the fluidization chamber with the fluidization gas to the chimney and allowing to increase the solids loading in the fluidization chamber at given solids feeding and fluidization gas flow rates. At sufficiently high chimney rotational speeds, particles entrained by the fluidization gas via the open end of the rotating chimney can be returned to the fluidization chamber by the action of the centrifugal force via the openings in between the chimney blades.

The concept of the rotating chimney was experimentally investigated using a dual step response technique. The responses of the rate of solids losses via the chimney and of the pressure drop over the fluidization chamber to step changes in the solids feeding rate were measured. This dynamic method allows obtaining data over the entire solids loading range from one single experiment. The influence of

the chimney rotational speed and the fluidization gas flow rate were measured.

At solids loadings below the theoretical maximum solids loading, the rate of solids losses via the chimney was found to be proportional to the solids loading and inversely proportional to the square of the chimney rotational speed. The fluidization gas flow rate was shown to have only a minor effect on the solids losses via the chimney. Nevertheless, at solids loadings below the theoretical maximum solids loading, the rate of solids losses via the chimney was found to decrease with increasing fluidization gas flow rate, whereas at solids loadings approaching the theoretical maximum, the rate of solids losses via the chimney was found to increase with increasing fluidization gas flow rate.

With increasing chimney rotational speed, the quasi steady state solids loading in the fluidization chamber at given solids feeding and fluidization gas flow rates, i.e. the solids loading at which the rate of solids losses via the chimney compensates the solids feeding rate, increases, up to the theoretical maximum. The latter is easily approached at chimney rotational speeds such that the rotational speed of particles at contact with the chimney is higher than the average particle bed rotational speed. At the given chimney rotational speed and solids feeding rate, the quasi steady state solids loading in the fluidization chamber is seen to decrease slightly with increasing fluidization gas flow rate.

The chimney rotational speed allowing to control the rate of solids losses via the chimney at given solids loading in the fluidization chamber and fluidization gas flow rate, the rotating chimney can eventually be used to control the average particle residence time in the fluidization chamber.

Different flow regimes were observed and mapped, i.e. channeling, slugging, and a stable rotating fluidized bed. The flow regime was found to depend mainly on the solids loading in the fluidization chamber, the chimney rotational speed and the fluidization gas flow rate only having a minor effect. Channeling occurs at the lowest solids loadings. At somewhat higher solids loadings, slugging occurs. Over a broad, high solids loading range, however, a stable rotating fluidized bed can be obtained. Increasing the chimney rotational speed allows to build up more easily, that is, at lower solids feeding rates, a sufficiently high solids loading in the fluidization chamber. Furthermore, with increasing chimney rotational speed or fluidization gas flow rate, the minimum solids loading required to obtain a stable rotating fluidized bed slightly decreases.

In the channeling and slugging regime, the pressure drop over the fluidization chamber was shown to be independent of the solids loading in the fluidization chamber, most of the fluidization gas bypassing the particles, and to be proportional with the fluidization gas flow rate. In the stable rotating fluidized bed regime, however, the pressure drop over the fluidization chamber and the pressure drop over the rotating particle bed were observed to be proportional with the solids loading in the fluidization chamber, as well as with the fluidization gas flow rate. For the fluidization chamber design and the 1G-Geldart D-type particles used in the present work, radial fluidization of the rotating particle bed is almost absent. The injection of the fluidization gas in the fluidization chamber is responsible for about 65–80% of the pressure drop over the fluidization chamber, whereas the radial pressure drop over the rotating particle bed is responsible for about 5–6% of the pressure drop over the fluidization chamber and the tangential pressure drop in the rotating particle bed is responsible for about 10–20% of the pressure drop over the fluidization chamber. The contribution of the chimney rotational motion to the pressure drop over the fluidization chamber logically depends on the chimney rotational speed, but is, under the conditions investigated, at its maximum still about one order of magnitude smaller than the contribution of the injection of the fluidization gas in the fluidization chamber.

The overall behavior of the rotating fluidized bed (average particle bed rotational speed, flow regime,...) does not seem to be much influenced by the action of the rotating chimney. In that sense, the observations on the different flow regimes (channeling, slugging, stable rotating fluidized bed) and on the pressure drop over the fluidization chamber and over the rotating particle bed as a function of the solids loading and the fluidization gas flow rate may also be of interest to rotating fluidized beds in a static geometry.

Finally, the advantages of using a rotating chimney for rotating fluidized beds should be emphasized. With increasing chimney rotational speed, the rate of solids losses via the chimney at given solids loading in the fluidization chamber and fluidization gas flow rate drastically reduces. As such, increasing the chimney rotational speed allows to increase the solids loading in the fluidization chamber at given solids feeding and fluidization gas flow rates. At sufficiently high chimney rotational speeds, the theoretical maximum solids loading in the fluidization chamber can be easily approached and the rate of solids losses via the chimney becomes almost independent of the solids loading in the fluidization chamber over a broad solids loading range. Alternatively, at given solids loading and fluidization gas flow rate, the chimney rotational speed can be used to control the average particle residence time in the fluidization chamber.

## Acknowledgments

Luc Wautier at UCL is greatly acknowledged for the technical realization of the project, for his help with the experiments, and for the helpful discussions.

## Notation

$d$ = diameter [m]
$F$ = force per cubic meter particle bed [N/m$^3$ particle bed]
$G$ = fluidization gas flow rate [Nm$^3$/h]
$\tilde{G}$ = fluidization gas flow rate [m$^3$/s]
$H$ = rotating fluidized bed height (radially) [m]
$L$ = fluidization chamber length [m]
$P$ = gas phase pressure [Pa]
$r$ = radius [m]
$s$ = slip factor
$R$ = outer radius [m]
$u$ = gas phase velocity [m/s]
$v$ = solids velocity [m/s]

### *Greek letters*

$\beta$ = drag coefficient [kg/(m$^3$ s)]
$\varepsilon$ = volume fraction
$\phi$ = sphericity factor
$\mu$ = viscosity [Pa s]

$\omega$ = rotational speed [rpm] (rotations per minute)
$\tilde{\omega}$ = rotational speed [rad/s] (radians per second)
$\rho$ = density [kg/m$^3$]

### *Subscript/superscript*

c = chimney
g = gas phase
gs = gas–solid
p = particle
rad = radial
s = solids
sc = particle-chimney
tan g = tangential

## Literature Cited


1. Kunii D, Levenspiel O. *Fluidization Engineering*, 2nd ed. Chemical Engineering Series. Boston: Butterworth-Heinemann, 1991.
2. Liu YA, Hamby RK, Colberg RD. Fundamental and practical developments of magnetofluidized beds—a review. *Powder Technol.* 1991;64:3–41.
3. Kroger DG, Levy EK, Chen JC. Flow characteristics in packed and fluidized rotating beds. *Powder Technol.* 1979;24:9–18.
4. Chevray R, Chan YNI, Hill FB. Dynamics of bubbles and entrained particles in the rotating fluidized bed. *AIChE J*. 1980;26:390–398.
5. Fan LT, Chang CC, Yu YS, Takahashi T, Tanaka Z. Incipient fluidization condition for a centrifugal fluidized bed. *AIChE J*. 1985;31: 999–1009.
6. Saunders JH. Particle entrainment from rotating fluidized beds. *Powder Technol*. 1986;47:211–217.
7. Chen Y-M. Fundamentals of a centrifugal fluidized bed. *AIChE J*. 1987;33:722–728.
8. Ahmadzadeh A, Arastoopour H, Teymoour F. Rotating fluidized bed an efficient polymerization reactor. *Proceedings of AIChE Annual Meeting 2005*. Cincinnati, OH, USA, 2005.
9. Qian G-H, Bagyi I, Burdick IW, Pfeffer R, Shaw H, Stevens JG. Gas-solid fluidization in a centrifugal field. *AIChE J*. 2001;47:1022–1034.
10. Quevedo J, Pfeffer R, Shen Y, Dave R, Nakamura H, Watano S. Fluidization of nanoagglomerates in a rotating fluidized bed. *AIChE J*. 2006;52:2401–2412.
11. Quevedo JA, Nakamura H, Shen Y, Dave RN, Pfeffer R. Fluidization of nanoparticles in a rotating fluidized bed. *Proceedings of AIChE Annual meeting 2005*. Cincinnati, OH, USA, 2005.
12. De Wilde J, de Broqueville A. Rotating fluidized beds in a static geometry: experimental proof of concept. *AIChE J*. 2007;53:793–810.
13. de Broqueville A. Catalytic polymerization process in a vertical rotating fluidized bed: Belgian Patent 2004/0186, Internat. Classif.: B01J C08F B01F; publication number: 1015976A3.
14. de Broqueville A, De Wilde J. Device and method for injecting fluid into a rotating fluidized bed, International application number: PCT/EP2007/053941 (F-995-WO), Publication number: WO/2007/122211, European and United States of America patent, 2007.
15. Ergun S. Fluid Flow through packed columns. *Chem Eng Prog*. 1952;48:89.


*Manuscript received Oct. 17, 2007, and revision received Apr. 20, 2008.*